Comparative Transcriptome and DNA Methylation Analysis in Temperature-Sensitive Genic Male Sterile Wheat BS366

Yong-jie Liu
Beijing Academy of Agriculture and Forestry Sciences
Dan Li
Beijing Academy of Agriculture and Forestry Sciences
Jie Gong
Beijing Academy of Agriculture and Forestry Sciences
Yong-bo Wang
Beijing Academy of Agriculture and Forestry Sciences
Zhao-bo Chen
Beijing Academy of Agriculture and Forestry Sciences
Bin-shuang Pang
Beijing Academy of Agriculture and Forestry Sciences
Xian-chao Chen
Beijing Academy of Agriculture and Forestry Sciences
Jian-gang Gao
Beijing Academy of Agriculture and Forestry Sciences
Wei-bing Yang
Beijing Academy of Agriculture and Forestry Sciences
Feng-ting Zhang
Beijing Academy of Agriculture and Forestry Sciences
Yi-miao Tang
Beijing Academy of Agriculture and Forestry Sciences
Chang-ping Zhao
Beijing Academy of Agriculture and Forestry Sciences
Shi-qing Gao (gshiq@126.com)
Beijing Academy of Agriculture and Forestry Sciences

Research Article

Keywords: Triticum aestivum L., Pollen, Temperature-sensitive genic male sterility (TGMS), Transcriptome, DNA methylation

Posted Date: July 7th, 2021

DOI: https://doi.org/10.21203/rs.3.rs-582568/v1

Version of Record: A version of this preprint was published at BMC Genomics on December 1st, 2021. See the published version at https://doi.org/10.1186/s12864-021-08163-3.

Abstract

Background: Known as the prerequisite component for the heterosis breeding system, the male sterile line determined the hybrid yield and seed purity. Therefore, a deep understanding of the mechanism and gene network that leads to male sterility is crucial. BS366, a temperature-sensitive genic male sterile (TGMS) line, were male sterile under cold condition (12℃ with 12 h daylight) but fertile under normal temperature (20℃ with 12 h daylight).

Results: During the meiosis, BS366 was defective in forming tetrad and dyad due to the abnormal cell plate. During the pollen development, unusual vacuolated pollen that cannot accumulate starch grains at the binucleate stage was also observed. Transcriptome analysis revealed that genes involved in the meiotic process like sister chromatid segregation and microtubule-based movement were repressed, while genes involved in DNA and histone methylation were induced in BS366 under cold condition. MethylRAD was used for a reduced DNA methylation sequencing for BS366 under both cold and control conditions. The differentially methylated sites (DMSs) located in the gene region were mainly involved in carbohydrate and fatty acid metabolism, lipid metabolism, and transport. Genes differentially and methylated were mainly involved in cell division.

Conclusions: These results indicated that methylation of genes involved in carbon metabolism or fatty acid metabolism would contribute to the male sterility in BS366, which will provide a novel insight into the molecular mechanism of wheat male sterility.

Background

Known as an environmentally sustainable and safe way to feed the increasing global population, heterosis has been shown to increase the crop yield by 3.5%-15% [1]. It has also been successfully implemented in crops like maize [2] and rice [3]; however, hybrid wheat is only grown on less than 0.2% of the global acreage [1]. Although male sterility is an unfavorable trait for the individual plant, it played critical roles for utilization of heterosis by facilitating hybrid breeding [4]. Male sterility can be classified into cytoplasmic male sterility (CMS) and genic male sterility (GMS). CMS was controlled by cytoplasmic genes and can be restored by nuclear restorer gene(s). GMS was controlled by nuclear genes. It would be male sterile under restrictive environmental conditions and fertile under permissive conditions [4]. Up to now, two recessive mutants (*ms1* and *ms5*) and three dominant mutants (*Ms2*, *Ms3*, and *Ms4*) were identified in wheat [5-9]. *Ms1* encodes a phospholipid-binding protein [10, 11]. *Ms2* was the first cloned dominant male GMS gene, and has been widely used for wheat breeding [12, 13]. Known as a glycosylphosphatidylinositol anchored lipid transfer protein, *Ms5* was required for normal pollen exine development [14].

Anther and pollen development have been widely studied in *Arabidopsis* [15], rice [16, 17], maize [2] and wheat [18]. Pollen development in those species involves similar key stages, which include microsporogenesis and male gametogenesis stages [2, 19, 20]. During the microsporogenesis stage, the archesporial cells differentiate into microspore mother cells (MMCs), which finally underwent meiosis to generate microspores. During cytokinesis in plants, the parent cell divided into two daughter cells via physical insertion of a membranous cell plate [21]. Phragmoplast, a specialized cytoskeletal array, expands centrifugally during cytokinesis and directs Golgi-derived vesicles to form the developing cell plate. This process involves extensive protein secretion and membrane trafficking toward the plane of cell division [22]. During the male gametogenesis stage, the vacuolated microspore undergoes twice mitosis to produce a larger vegetative cell and a pair of sperm cells [23].

DNA methylation is a kind of epigenetic modification existed in plant genomes. Epigenetic modification of a single locus would result in heritable morphological variations without DNA sequence alteration [24, 25]. It has been reported that DNA methylation participated in many plant development processes, including flower tissue development, pollen fertility, fruit ripening, and stress responses [26-30]. DNA methylation in plant occurs at the symmetrical CG, CHG, and the asymmetrical CHH (H represents A, T, or C) contexts [31]. CHG and CHH DNA methylation usually participate in the heterochromatin formation and gene expression silencing, but the methylation sites in CG context were mainly in the gene bodies [32, 33]. Male reproductive organs are more sensitive to damage from environmental change than vegetative organs [34]. There is increasing evidence that epigenetic regulation is essential for male sterility in plants. It has been reported that DNA demethylation was found in the vegetative and sperm cells, which reactivated the transposable elements (TEs) and transposition in *Arabidopsis* [35]. In recent studies, changes were detected in the levels of DNA methylation in cotton (*Gossypium hirsutum*) anthers under high temperature (HT) in both HT-tolerant and HT-sensitive cotton cultivars [29, 30]. In rice, the methylation in the putative promoter region of LDMAR reduced its transcription level specifically under long-day conditions, which resulted in premature programmed cell death (PCD) in developing anthers, thus causing photoperiod-sensitive male sterility [36]. In rice PTGMS line PA64S, the DNA methylation patterns were compared under sterile and fertile environments and the hypermethylated *BIM2* gene may suppress downstream genes in brassinosteroid signaling pathway and thus affect the male fertility in PA64S [37].

Known as the prerequisite component for the heterosis breeding system, male sterile line determined the hybrid yield and seed purity. Therefore, a deep understanding of wheat fertility and the mechanisms and gene networks that lead to male sterility are needed. Up to now, three wheat male sterile genes including *TaMs1*, *TaMs2*, and *TaMs5* have been cloned; however, no study focusing on cloning of temperature or photo-sensitive male sterile genes have been reported in wheat so far. In this study, a transcriptome and a reduced methylome sequencing were carried out for BS366 and J411 (Jing411, a normal inbred line) under male sterile (12℃ with 12 h daylight) and fertile conditions (20℃ with 12 h daylight). The differentially expressed and methylated genes functioning in the cell division, carbohydrate and lipid metabolism pathways were identified. Our study will provide a novel insight into the role of DNA methylation in the male sterility in wheat.

Results

Anther and pollen development was defective in BS366 under cold condition

BS366 is a thermo-sensitive male genic sterile line. It was male sterile under 12℃, and male fertile under 20℃ with 12 h daylight. The fertile anthers were dark yellow, and its spherical pollen could be darkly stained by I_2-KI, indicating much starch accumulation (Fig. 1a and b). The sterile anthers were short, light yellow and its pollen cannot be stained by I_2-KI compared with the normal one (Fig. 1c and d). No difference was observed between the pollen mother cells (PMCs) of sterile and fertile BS366. Their PMCs divided normally to form microspore mother cells (Fig. 2a and e). The meiosis appeared to be normal in BS366 under control condition. Dyad and tetrad formed normally in the control (Fig. 2b and c), while some of the dyad and tetrad were abnormal in the sterile BS366. During the formation of the sterile pollen, some dyad was absent of a smooth cell plate at telophase I (Fig. 2f). A more severe defection was observed during the formation of the tetrad, with a serious defective of the cell plate at the telophase II (Fig. 2g), which resulted in an abnormal tetrad and cannot release uninucleate pollen grains. There was no obvious difference in the early (Fig. 2d and h) and middle uninucleate stage (Fig. 2i and m), but a significant difference was observed at the vacuolated stage (Fig. 2j and n). The pollen grains in sterile BS366

shrank at the vacuolated stage. As the starch accumulates inside the microspore, the vacuole diminishes gradually in the fertile pollens (Fig. 2k). At the mature pollen stage, pollen grains in fertile BS366 were full of starch (Fig. 2l). In the sterile pollen, no starch accumulates and a smaller nucleus without generative and vegetative cells was observed (Fig. 2o). The sterile pollens were vacuolated (Fig. 2p) and cannot be stained blue with 1% I_2-KI solution at the mature stage (Fig. 1d).

To characterize the histological differences between fertile and sterile anthers, transverse section of anthers embedded in paraffin and stained with safranin O-fast green was observed. The sporogenous cells, epidermis, endothecium, middle layer, and tapetum showed no difference between anthers from sterile and fertile BS366. No abnormal structures were observed at the pre-callose stage (Fig. 3a and e) and meiotic stage (Fig. 3b and f). Compared with the fertile anther (Fig. 3c and d), a serious defect of cell plate in the dyad and tetrad was observed (Fig. 3g and h). At the vacuolated stage, round and vacuolated microspores were observed (Fig. 3i and m). Compared with the fertile BS366 (Fig. 3j), sterile microspores were swollen and became less vacuolated and collapsed (Fig. 3n). The fertile pollens started to accumulate starch grains at the binucleate stage (Fig. 3k), while little starch grains were observed in the sterile pollen (Fig. 3o). At the mature stage, the fertile anther locule was full of mature pollen grains and anther dehiscence occurs, leaving only the epidermis and endothecium layers (Fig. 3l). However, the sterile middle layer and endothecium became abnormally expanded and thicker, and the microspore had an irregular appearance. In particular, the endothecium near the connective tissues expanded, and the pollen disintegrated into debris (Fig. 3p).

Profiling the transcriptome of BS366 and J411 under different conditions

To gain an overall knowledge of male sterile under the low temperature and male fertile under normal temperature, transcriptome analysis was implemented for BS366 and J411. Young spikes of BS366 and J411 from low and normal temperature of different anther development stages, including dyad, tetrad, early uninucleate stage, vacuolated stage were pooled together to prepare cDNA libraries, respectively. All the libraries were subjected to RNA sequencing analysis using the Illumina Hiseq 2500 platform. Transcriptome sequence data for all samples can be found in the National Genomics Data Center (https://bigd.big.ac.cn/) under the accession number CRA003366. After filtering and quality control of the raw reads, a total of 910,342,786 clean reads were generated, with an average of 96,761,244 reads per sample. RNA-seq sequences were mapped to the wheat assembly genome (IWGSC RefSeq v1.0) using HISAT (v2.0.6) [38] and the underlying gene annotation was used to assign reads to respective gene models. Finally, 85.07% (774,089,948/910,342,786) of the reads were mapped to the reference genome, of which, 86.16% (666,921,316) reads were uniquely mapped (Table 1). The correlation between biological replicates varied between 0.87-0.94 for BS366 and J411 under fertile and sterile conditions (Additional file 1: Figure S1), which indicates a good replication of those samples.

The differentially expressed genes and function analysis

To characterize the expression changes of putative candidate genes involved in male sterility under the cold condition in BS366, differentially expressed genes (DEGs) were calculated. Fragments per kilo base of exon model per million mapped reads (FPKM) was used to estimate the transcript expression levels in all samples. In BS366, there are 7879 genes expressed, among which 4438 genes were expressed in normal and 6879 genes expressed under the cold condition. Totally 7415 genes were expressed in J411, with 4573 genes expressed in normal and 6438 genes expressed under the cold condition. The expressed genes in BS366 and J411 under normal/cold conditions were about the same. DEGs in each comparison were identified by DEseq2 using a threshold P-value <

0.05 and a fold change ≥ 2 [39]. 2507 genes were identified as differentially expressed in this study, with 1672 in BS366 and 657 in J411 between control and cold conditions (Fig. 4a and c). There were 301 DEGs under the control condition and 914 DEGs under the cold condition between BS366 and J411. As shown in Fig. 4a, there were 919 genes exclusively differentially expressed between cold and control conditions in BS366.

To illustrate the alternation of transcriptome accompany the change of temperature, the DEGs were classified as up- or down-regulated in the cold condition and/or BS366 according to their expression levels. Finally, 1068 up-regulated genes and 604 down-regulated genes were found in sterile BS366. In J411, 193 up-regulated and 464 down-regulated genes were identified under sterile condition compared with the control. Compared with J411, there are 125 up-regulated and 176 down-regulated genes in BS366 under control condition and 579 up-regulated and 335 down-regulated genes in BS366 under cold condition (Fig. 4b). These results indicate a more rigorous transcriptome change in BS366 between cold and control conditions than J411.

The exclusive DEGs in BS366 between cold and control conditions will undoubtedly contribute to the male sterility in sBS366. Thus, the Gene Ontology (GO) analysis was performed for those BS366-specific DEGs. Among the top 20 go terms of molecular function, structural molecule activity, binding activities like RNA binding, heterocyclic compound binding, organic cyclic compound binding, mRNA binding, nucleic acid binding, protein binding were significantly represented. In addition to the go terms mentioned above, microtubule binding, cytoskeletal protein binding, microtubule motor activity, tubulin binding, motor activity were also significantly represented (Additional file 2: Table S1). In the biological process category, the top three go terms were DNA conformation change, chromosome organization, and translation which have been reported to be common for male sterility in other plants. Other biological processes including DNA unwinding involved in DNA replication, mitotic cell cycle process, microtubule-based process, chromatin organization sister chromatid segregation movement of cell or subcellular component, microtubule-based movement, chromosome segregation were also significantly represented. The epigenetic regulation like histone methylation, negative regulation of gene expression, epigenetic, DNA methylation on cytosine, and histone H3-K27 methylation were enriched in those BS366-specific DEGs (Additional file 2: Table S1). Compared with BS366 enriched biological processes in DEGs specific for BS366 between cold and control conditions, there are only four significantly (P-value□0.05) enriched biological processes in J411. Those processes include photosynthesis, light reaction protein-chromophore linkage, generation of precursor metabolites, energy calcium ion transmembrane transport and photosynthesis (Additional file 2: Table S1). All those BS366 specific DEGs enriched processes indicated that it is a comprehensive dynamic molecular network to cause male sterility in BS366.

Co-expression module analysis of all the differentially expressed genes

All the 2507 DEGs between different conditions and/or materials were used to construct co-expression modules. Finally, 2329 genes were assigned to 12 expression modules, for which the gene number ranged from 35 (tan) to 1022 (turquoise) (Additional file 1: Figure S2 and S3). As shown in Fig. 5, most of DEGs (1023, 43.88%) were assigned to the turquoise module, in which all the genes exhibited lower expression level in fBS366, fJ411, and sJ411 but a higher expression level in sBS366. Compared with genes in the turquoise module, 142 genes in the red module exhibited an opposite expression pattern. Only genes in sBS366 expressed at high levels compared with other samples (Fig. 5a and c).

To gain an overall interview of the genes assigned to the two opposite modules, GO analysis was implemented for either module respectively. In the red module, genes were enriched in biological processes related to meiotic sister

chromatid segregation and cohesion, mRNA cleavage involved in gene silencing, and microtubule-based movement (Fig. 5b and Additional file 3: Table S2). In the turquoise module, genes were mainly enriched in processes related to DNA methylation and histone modification, microtubule-related processes and movement. Genes assigned to the molecular function were significantly enriched in methyl-CpG binding, histone-binding, DNA (cytosine-5)-methyltransferase activity, 5-methyltetrahydropteroyltriglutamate-homocysteine S-methyltransferase activity, and histone methyltransferase activity (H3-K4 specific). In the cellular component category, genes in the MCM complex, cell wall, tubulin complex, microtubule, and mitotic spindle were significantly enriched. In the molecular function, those genes were enriched in microtubule motor activity, DNA (cytosine-5)-methyltransferase activity, microtubule binding, histone methyltransferase activity (H3-K4 specific), calcium-transporting ATPase activity, 1, 3-beta-D-glucan synthase activity, methyl-CpNpG binding, methyl-CpNpN binding, methyl-CpG binding, methylated histone binding, and methylation-dependent protein binding (Fig. 5d and Additional file 4: Table S3).

Similar to DNA methylation, many histone constitution- and modification-related genes were found in the turquoise module. A total of 68 histone constitution genes (such as Histone H1, Histone H2A, Histone H2B, Histone H3) showed expression peaks in sBS366 (Additional file 1: Fig S4a). Similarly, eight genes involved in histone modification also showed higher expression levels in sBS366 than in other samples (Additional file 1: Fig S4b). Those genes encoding proteins like Histone-lysine N-methyltransferase ATXR5, histone-lysine N-methyltransferase, putative histone-lysine N-methyltransferase ATXR3, Histone-lysine N-methyltransferase H3 lysine-9 specific SUVH5, histone deacetylase HDAC2. Seven genes encoding homologies of DNA (cytosine-5)-methyltransferase 1 (DRM1) or DNA (cytosine-5)-methyltransferase 1B in *Aegilops tauschii* or *Triticum Urartu* showed higher expression levels in sBS366 compared with other samples (Additional file 1: Fig S4c). Based on the above results, we may conclude that induced expression of DNA methylation-related genes are likely to cause the higher methylation level in sBS366; the higher expression of histone constitution genes in sBS366 may allow anthers to maintain DNA stability in sBS366. These results indicate that epigenetic modifications, particularly the DNA methylation and histone modifications, were involved in the anther development under the low temperature conditions.

Expression validation of differentially expressed genes in transcriptome data

Finally, 19 DEGs in BS366 between control and cold conditions were selected for validation using the real-time qRT-PCR. The Pearson's correlation coefficient between data generated from the two platforms was very high (R^2 = 0.93), indicating that RNA-seq analysis generated dependable data (Additional file 1: Fig S5).

Genome-wide DNA methylation in BS366 and J411 under two conditions

The exclusive DEGs involved in DNA methylation and histone modification suggested DNA methylation may involve in the male sterility of BS366. To delineate the role of DNA methylation in pollen sterility, MethylRAD analysis [40], a cost-efficient DNA methylation profiling method was used to characterize the cytosine methylation patterns of spikes. Eight samples for BS366 and J411 under both cold and control conditions were sampled and prepared for the MethylRAD sequencing library. Totally 1,089,514,960 raw reads were obtained, of which 364,356,240 (33.44%) enzyme digested reads were identified. There are 359,562,630 enzyme digested reads mapped to the reference wheat genome (IWGSC RefSeq v1.0), and of which, 31,327,447 reads were uniquely mapped (Table 2). MethylRAD sequence data for all samples can be found in the National Genomics Data Center (https://bigd.big.ac.cn/) under accession number CRA003366. In this analysis, only the uniquely mapped reads were retained to measure the methylation level of loci.

Using the MethylRAD method, we can analyze the DNA methylation at the CG and CHG (H=T or A) sites in the whole genome. As shown in Fig. 6 and Additional file 5: Table S4, there are 3,238,375 CCGG and 1,936,460 CCWGG sites in sBS366, 3,473,022 CCGG and 2,069,354 CCWGG sites in fBS366. In J411, there are 3,167,380 and 1,893,560 CCGG and CCWGG sites in sJ411, 3,191,535 and 1,971,193 methylated CCGG and CCWGG sites in fJ411, respectively. The methylation profiles within genes including promoter, exon, and intron were analyzed for four samples. Clearly, the CCGG context showed a higher methylation level than the CCWGG context in the gene region. However, the distribution patterns of methylated sites at different elements of genomes were similar for CCGG and CCWGG sites. The CCGG and CCWGG sites in the intergenic regions were easily methylated, followed by the upstream 2000 bp region of transcription start sites (TSS2000), intron, exon, the Utr3prime, and Utr5prime regions (Fig. 7a and 7b). According to the method of MethylRAD, we compared the methylation profiles of sites in the up- and down-stream 2000 bp of TSS, TSS and the gene body. We found that the methylation context was higher for CCGG than CCWGG for the above three characters. The methylation level was higher in the upstream 2000 bp than that in the gene body, and TTS region for both CCGG and CCWGG context. The methylation levels were a little higher for the TSS region than that in the gene body region for both CCGG and CCWGG context (Fig. 7c).

The differentially methylated sites and functional analysis

To further identify the function of methylation changes among gene features in response to cold stress, the differentially methylated sites (DMSs) in BS366 and J411 between different conditions were characterized using the criteria of |log 2FC| >1 and P-value < 0.05. Totally 36,392 CCGG and 23,787 CCWGG loci were detected as differentially methylated in BS366 between cold and control conditions. More DMSs were detected in BS366 than in J411 for both CCGG and CCWGG sites between two conditions (Fig. 8a). The DMSs were further divided into hyper-methylated and hypo-methylated sites. More DMSs were detected in the BS366 between cold and control conditions than that in J411for both hyper-methylated and hypo-methylated sites. There are 17,715 and 9966 hyper-methylated CCGG and CCWGG sites in sBS366 and 18,677 CCGG and 13,821 hypo-methylated CCWGG sites in sBS366. There are 9,448 CCGG and 7,528 CCWGG sites hyper-methylated in sJ411; there are 18,327 CCGG and 12,187 CCWGG sites hypo-methylated in sJ411 (Fig. 8b). We further inspected DMSs distribution in the genome elements and found that, the majority of the DMSs located in the intergenic region (92.01-97.39%), following by the exon, intron, upstream, utr3prime, and utr5prime region for CCGG DMS; the CCWGG DMSs were mainly located on the intergenic region upstream, intron, exon region (Additional file 1: Fig S6). To explore the pathways that are important for male sterility in BS366 response to the cold condition, the DMSs-specific for BS366 were annotated to the reference pathways in the KEGG. In this analysis, 1130 CCGG DMSs and 633 CCWGG DMSs assigned to 1591 genes were retained (Fig. 9a). KEGG enrichment analysis revealed that pathways including phospholipase D signaling pathway, fatty acid biosynthesis, fatty acid degradation, and peroxisome were significantly enriched (Fig. 9b). All those results indicated that pathways involved in the fatty acid metabolism, phenylpropanoid biosynthesis, and phospholipase D signaling pathway may be regulated by the DNA methylation to participate in the male sterility in BS366 under cold condition. In the GO analysis of the DMSs specific for BS366, biological processes including carbohydrate transport, oxylipin biosynthetic process, positive regulation of transcription from RNA polymerase II promoter, and lipid transport were also significantly represented (Additional file 6: Table S5).

Genes differentially expressed and methylated between different conditions in BS366

The DMSs in the methylome and DEGs in the transcriptome sequencing were integrated to investigate the role of DNA methylation in gene expression. Genes that are differentially expressed and methylated in BS366 under

different conditions were identified. Finally, 49 DMSs in the methylome sequencing located in 45 DEGs in the transcriptome sequencing were found. Those genes were classified into four categories, 1）eight genes with lower methylation and expression levels; 2) 15 genes with lower methylation levels but higher expression levels; 3) five genes with higher methylation levels but lower expression levels and 4) 21 genes with higher expression and methylation levels in BS366 under cold condition (Fig. 10). Among those sites, 13 were located in the upstream region, eight located in the intron region, and 36 located in the exon region.

For instance, a gene encoding AGO1d protein (TraesCS7A02G557400) expressed higher but hypo-methylated in sBS366 than fBS366. A gene encoding AGO4, partial protein (TraesCS1A02G445500) expressed and methylated higher in sBS366 than fBS366. A homology gene (TraesCS1B02G179900) of *DNA-directed RNA polymerase I subunit 2* in *Brachypodium distachyon* and a homology gene (TraesCS6D02G113900) of *DNA-directed RNA polymerase II subunit RPB1-B* in *Aegilops tauschii* were hyper-methylated in sBS366 than fBS366. However, the methylation tendency of these two genes differed, with the former down-regulated and the latter up-regulated in sBS366. A homology gene (TraesCS7D02G206700) of *Chromatin structure-remodeling complex subunit snf21* in *Aegilops tauschii* was up-regulated but hypo-methylated in sBS366. Gene encoding sister chromatin cohesion protein PDS5-like protein B (TraesCS7A02G215200) was up-regulated and hyper-methylated in sBS366. Two genes encoding histone proteins: one homology to putative histone H2AXb in *Aegilops tauschii* (TraesCS5A02G098300) and H2A3 protein (TraesCS1B02G048900) up-regulated but hypo-methylated in sBS366. One gene encoding a ribosomal protein L19 (TraesCS2D02G092800) was up-regulated and hyper-methylated in sBS366 (Fig. 10).

Pyrosequencing validation of the differentially methylated sites

We selected the AGO1d (TraesCS7A02G557400) *and* H2A3 encoding gene (TraesCS1B02G048900) for the expression and methylation level validation. Four sites were chosen for the validation of methylation level in BS366 under cold and control conditions using bisulfite sequencing. The expression and methylation level correlated well with that in the sequencing data. The expression of *AGO1d* gene was higher under the cold condition (Fig. 11a), but four CG sites in the gene were found to hyper-methylated in BS366 under control condition in the *AGO1d* gene (Fig. 11b and c). For the H2A3 encoding gene, the expression level was higher in BS366 under the cold condition, but the methylation level was higher for CG, CHG, and CHH context (Fig. 12 a, b). As shown in Fig. 12c, four CG sites were hyper-methylated in the control condition than in the cold condition. Other validated DMSs were shown in Additional file 1: Figure S7, S8, and S9, all correlated well with the MethylRAD sequencing data.

Discussion

Known as the prerequisite component for the heterosis breeding system, the male sterile line directly determined the hybrid seed purity and yield. Therefore, a deep understanding of wheat sterility and the mechanisms and gene networks that lead to male sterility is needed. In this study, a TGMS line (BS366) and normal inbred lines (J411) were used to explore the underlying male sterile mechanisms. BS366 were sterile under cold condition. It has smaller anther and sterile pollens with no starch accumulation. Histological observation revealed that the unusual formation of dyad and tetrad during meiosis and of vacuolated stage pollen were also observed. All these lead to the male sterile of BS366 pollen under the cold condition. A transcriptome and reduced methylome sequencing were carried out for BS366 and J411 under cold and control conditions. All the DEGs and DMSs were identified and pathways involved in cell division, carbohydrate, and lipid metabolism were found to be correlated with the

male sterile of BS366. We also found that carbohydrate transport, oxylipin biosynthetic process, positive regulation of transcription, and lipid transport were differentially methylated in BS366 under cold and control conditions.

The cell division was impaired in BS366 at the anaphase in meiosis I and II

During cytokinesis in plants, the parent cell divided into two daughter cells via a physical insertion of a membranous cell plate, which involves a de novo construction of a cell wall [21, 41, 42]. The phragmoplast, known as a plant-specific cytoskeletal configuration, involves in the cell wall assemble at the late anaphase [43]. Phragmoplast in plants was composed of microtubules (MTs), microfilaments, motor proteins, and several regulators [43-47]. MTs in phragmoplast were organized as two opposite sets, which overlap at the equator [48, 49]. Golgi-derived vesicles are responsible for the transportation and fusion of the cell wall containing materials to this site to form the cell plate [22]. Finally, the cell plate assembled towards the cell edges in an actin-dependent process [50, 51].

The histological observation indicated that disrupted dynamic organization of phragmoplast microtubules and deposition of the cell plate, causing defective cytokinesis during meiosis I [52]. The BS366 and BS366-specific DEGs are enriched in biological processes including microtubule-based processes, cytokinesis by cell plate formation, cytoskeleton-dependent cytokinesis, and microtubule-based movement. As indicated above, the phragmoplast initiated cell plate formation was impaired in this study (Figure 2 and 3). The significant enrichment of those processes corresponds well to the histological observation. We further inspected the DEGs involved in those processes and found that those genes including tubulin-relate proteins, kinesin related proteins encoding genes, MT-associated proteins 65 (MAP65) related proteins encoding genes, MCM-related genes (Additional file 7: Table S6). MTs were assembled by the heterodimers of alpha- and beta-tubulin GTPases in a head-to-tail manner, which serves as tracks for transport and frameworks for the spindle assemble and the phragmoplast formation [53, 54]. Studies involved in genetic analysis have shown that β-tubulin is essential for MT organization in *A. thaliana* [55, 56]. We also found that seven α-tubulin and eight β-tubulin encoding genes were differentially expressed between sBS366 and fBS366, all of which expressed at higher levels in sBS366 than fBS366 (Additional file 7: Table S6). In this study, the abnormality expression pattern of those tubulin genes indicated that the structure and traffic in MTs may be impaired by the low temperature in BS366.

During cytokinesis, the cell plate biogenesis is accompanied by the vesicle fusion at its margins and the dynamic turnover of microtubules [57]. This rapid turnover in plant cells must be initiated by MT-associated proteins (MAPs) [43]. In plant cytokinesis, MAP65 contributes to stabilize antiparallel microtubule overlaps in the phragmoplast [58, 59]. The MAP65-3 played a critical role in organizing the mitotic microtubule array during both early and late mitosis in all plant organs [60]. In this study, we screened all the orthologous of the nine MAP65 family genes in *Arabidopsis thaliana* [61], and identified 30 orthologous genes encoding MAP65 related protein. Among those genes, two (TraesCS7A02G223100, TraesCS7B02G190000) encoding orthologous of MAP65-1 and one (TraesCS7D02G224800) encoding orthologous of MAP65-2, one (TraesCS3A02G264600) encoding orthologous of MAP65-3 in *Arabidopsis* were differentially expressed between sBS366 and fBS366. All the four genes expressed at higher levels under cold condition compared with that under control condition (Additional file 8: Table S7). Kinesins were the largest cytoskeletal protein family in flowering plants. Cytoskeleton-based motors use the energy of release from ATP hydrolysis to move along MT tracks [62]. In *Arabidopsis thaliana*, Kinesin-12A and Kinesin-12B collaboratively play a critical role in the organization of phragmoplast microtubules. In the double mutant, the first post meiotic cytokinesis was abolished without the formation of a cell plate [63]. *OsKCH2* encodes a plant-specific kinesin-14 with an N-terminal actin-binding domain and a central motor domain. It specifically decorates

preprophase band microtubules in vivo and transports actin filaments along microtubules in vitro [64]. In this study, 12 genes encoding kinesin-related proteins were found differentially expressed in BS366 between cold and control conditions. Most of those genes were induced in sBS366 (Additional file 8: Table S7). We may conclude that lower temperature changed the expression of genes involved in cell plate formation which finally resulted in male sterility in BS366.

The carbohydrate and lipid metabolism pathways were altered in BS366 under cold condition

One reason for male sterility in BS366 was that the abnormal dyads and tetrads cannot successfully enter the development of microspores because of unable to generate uninucleate pollen grains; the other reason was the abnormality in the microspore development. As shown in Fig. 2 and 3, the pollen grains in sterile BS366 shrank at the vacuolated stage. No starch accumulates in the sterile pollen compared with the fertile pollen.

Carbohydrates were known to play important roles in anther developments via serving as nutrients and signals. Anthers cannot synthesis photosynthetic assimilates themselves [65]. Pollen develops inside the anther by immersed in the locular fluid which provides lipid and sugars generated from the degradation of tapetum [66]. At the late gametogenesis stage, the pollen became matured with a sign of starch accumulation, which functions as energy for seed germination [67]. In this study, genes involved in the carbohydrate metabolism and glycan biosynthesis and metabolism were exclusively differentially expressed between sBS366 and fBS366. Genes encoding proteins involved in the carbohydrate metabolism and transport like ADP-glucose pyrophosphorylase large subunit, beta-galactosidase 5, callose synthase 10, callose synthase 3, putative cellulose synthase A catalytic subunit 1 (UDP-forming), alpha-1, 4-glucan-protein synthase (UDP-forming), sucrose: fructan 6-fructosyltransferase, sucrose-phosphate synthase 9 putative xyloglucan endotransglucosylase/hydrolase protein 23, sugar transport protein 14, UDP-glycosyltransferase 85A2, xylan arabinosyl transferase were differentially expressed in BS366 between cold and control conditions (Additional file 9: Table S8).

Plant anthers are multilayered, multifunctional tissue. The tapetum provides sporopollenin and pollen coat constituents generated by lipid metabolism which is essential for exine formation [68]. Sporopollenin precursors, cutin, and wax were synthesized in the tapetum and translocated into the locule by ABCG transporters or lipid transport proteins to facilitate the anther cuticle and pollen exine development [69]. In rice and *Arabidopsis*, genes involved in the translocation of lipid have been identified. It has been reported that the ATP-binding cassette transport protein (ABCG15) and non-specific lipid transfer proteins (nsLTP) functions in sporopollenin precursor transportation [70, 71]. ABCG26 was involved in transporting components of sporopollenin and spermidines into the anther locule prior to the tapetum degradation [72]. Another analysis in *Arabidopsis* has shown that III-LTPs are involved in allocating and incorporating lipidic compounds to the pollen wall [73]. More recently, a wheat gene termed *TaMs1*, encoding a glycosylphophatidylinositol (GPI) LTP was demonstrated to be required for wheat male fertility [11, 74, 75]. It has been reported that male fertility in *Arabidopsis* is also influenced by jasmonates, fatty acid-derived products catalyzed by 13-lipoxygenases (13-LOXs). The lipoxygenase 2 (LOX2) was dispensable for fertility. The double mutant *lox3lox4* was male sterile, which showed indehiscent anthers and sterile pollen grains [76]. In this study, two LOX2, one LOX3, and a putative lipoyltransferase-like protein encoding genes were identified in the BS366-specific DEGs (Additional file 9: Table S8).

The BS366-specific DEGs were assigned to metabolism pathways like lipid metabolism. As indicated by the DNA methylation analysis, genes involved in lipid metabolism including oxylipin biosynthetic process, and lipid transport were differentially methylated. The KEGG analysis also showed that pathways like phospholipase D

signaling pathway, fatty acid biosynthesis, fatty acid degradation were significantly represented (Fig. 9). In this study, several genes involved in the transport of lipid or its derivate have been identified, including five ABC transporters, two Non-specific lipid transfer proteins (nsLTP), and one gene homologues to *ABCG26* in *Arabidopsis*. All those results indicated that the lipid metabolism and transport may be impaired by the low temperature which caused male sterility in BS366 (Additional file 9: Table S8).

DNA methylation may be involved in the male sterility in BS366

The development of reproductive organs directly determined the crop yield. Thus, understanding the manner of reproductive organs in front of temperature changes is of great importance. The male reproductive organs were more vulnerable to temperature damages than females and other organs, especially during the flowering stage and the young microspore stage [65, 77]. It has been reported that epigenetic regulation involves in transcriptional regulation in facing of abiotic stress like temperature challenges [78]. The DNA methylation level in normal cotton line was induced by high temperature (HT) but repressed in HT-sensitive cotton line [30]. It has also been reported that hyper-methylation were observed in the PTGMS line PA64S at a temperature higher than 23.5℃ under long-day condition [37]. In this study, the expression profile showed that processes related to DNA methylation were significantly enriched. Several *DRM1* or *DRM1*-related genes were exclusively differentially expressed between cold and control conditions in BS366 and assigned to the turquoise module (Supplementary Fig S3). Those *DRM1* genes all expressed at higher levels in sBS366 compared with fertile BS366. Thus, we may conclude that the temperature induced expression of DNA methylation genes may be involved in the male sterility in BS366. In the Methyl-RAD sequencing, differentially methylated sites located in genes assigned in the phospholipase D signaling pathway, fatty acid biosynthesis, fatty acid degradation were found (Fig. 9b). In the GO analysis of the DMSs specific for BS366, biological processes including carbohydrate transport, oxylipin biosynthetic process, lipid transport were also significantly enriched (Supplementary Table S6). It has been reported that the pollen wall development after the release of microspores from tetrad needs the involvement of fatty acid and lipid metabolism pathways. All those results suggested that DNA methylation may be involved in the male sterility in BS366 under the cold condition through the induced expression of DNA methyltransferase and suppression of fatty acid and lipid metabolism pathways.

Conclusions

Sterile BS366 has smaller anther and sterile pollens with no starch accumulation. Histological observation revealed that the formation of dyad and tetrad during meiosis and the vacuolated stage pollen were abnormal. Compared with the fertile BS366, genes involved in the biological processes including meiotic sister chromatid segregation and cohesion, mRNA cleavage involved in gene silencing, and microtubule-based movement were down-regulated, while genes involved in DNA methylation and histone modification were up-regulated in the sterile BS366. The DNA methylation sequencing revealed that the methylation level involved in carbohydrate transport, fatty acid metabolism, and lipid transport altered between sterile and fertile BS366. These results indicated a sign of DNA methylation involved in the temperature-sensitive genic male sterility in BS366.

Methods

Plant materials

The wheat temperature-sensitive genic male sterile (TGMS) line BS366 and the normal inbred line Jing411 (J411), both maintained at Beijing Engineering Research Center for Hybrid Wheat was used in this study. The plants were grown in plastic pots embedded in the ground in early October in the experimental farm of Beijing Academy of Agriculture and Forestry Sciences. The plants were vernalized naturally in the field and moved into the greenhouse. Before the five-leaf stage, plants of BS366 and J411 were selected and then randomly assigned to the cold and control temperature groups. The selected plants were grown in phytotrons (Koito, Tokyo, Japan) at 20℃ with a 12 h photoperiod for control temperature for the entire reproductive period. Cold temperature treatment was implemented with a temperature of 10℃ and a 12 h photoperiod for 10 days and then transferred to the control temperature environment for the entire reproductive period.

Phenotypic analysis of BS366

Photographs of the flower tissue for BS366 under cold and control environment were obtained using ZEISS SteREO Discovery. V20. To evaluate the pollen viability, cold and control anthers were separately crushed, stained with 1% odine-potassium iodide (I_2-KI) solution and photographed under the Olympus BX-53 microscope (Tokyo, Japan). For microspore and anther phenotype observation, anthers and spikelets of corresponding development stages during meiosis to mature pollen stage for BS366 under both control and cold conditions were collected and fixed in FAA solution (formaldehyde: glacial acetic acid: 50% ethanol =5: 5: 9). The anthers were separated from the young spikes, mashed with tweezers to release the pollens, and dyed with improved carbol fuchsin solution. The photographs of microspores and pollens were obtained using the Olympus BX-53 microscope (Tokyo, Japan). For the anther phenotype analysis, the anthers were in fixed FAA solution, removed from the FAA fixative, dehydrated in an ethanol series, and then embedded in Paraffin. Tissue sections were cut transversely from the wax-embedded anthers and stained using safranin O-fast green. The anther morphology was analyzed with a scanning electron microscope (HITACHI SU8100).

Sample preparation, RNA isolation and real-time qRT-PCR

Three main spikes from fifteen individuals of BS366 and J411 in the control and cold conditions from the meiosis stage to the vacuolated stage were pooled together respectively with two replicates. All samples were immediately frozen in liquid nitrogen and stored at −80 °C for RNA extraction. Total RNA from spikes of both lines under cold and control conditions were extracted using TRIzol Reagent (Invitrogen Corp., Carlsbad, CA). The concentration and quality of total RNA were determined with a Nanodrop spectrophotometer and 1% agarose gel electrophoresis and subjected to the transcriptome sequencing. For real-time qRT-PCR, cDNA was synthesized using the PrimeScript™ RT reagent Kit with gDNA Eraser (Takara). Differentially expressed genes were validated with a CFX96 Touch™ Real-Time PCR Detection System (Bio-Rad Laboratories, Hercules, CA, USA) using SYBR Green II (Takara). Expression levels of genes in samples were normalized using endogenous wheat 18S gene with primer sequences 5’-TGCTGGAATCGGAATAGTTGAG-3’ and 5’-ACTACGCAGGCTCATCAAACAG-3’. The relative expression levels were calculated using the $2^{-\Delta\Delta Ct}$ method. Primer sequences were designed using Primer3 input version 4.0.0 (http://primer3.ut.ee/) and listed in Additional file 10: Table S9.

Transcriptome sequencing and data analysis

All samples were sequenced using the Illumina HiSeq 2500 platform. Raw reads were filtered to remove low-quality reads containing more than 30% bases with Q-value < 20. After trimming low-quality bases (Q-value < 20) from the 5' and 3' ends of the remaining reads, the resulting high-quality clean reads in each sample were mapped to the

wheat reference genome (IWGSC RefSeq v1.0) using HISAT (v2.0.6) [38]. Only reads that were uniquely mapped to the reference genome were kept for further analysis. Fragments per kilobase of exon model per million mapped reads (FPKM) was used to estimate transcript expression levels. Differentially expressed genes (DEGs) in each comparison were identified by DEseq2 using a threshold P-value < 0.05 and a fold change ≥ 2 [39]. The identified DEGs were subjected to Gene Ontology (GO) [79] and Kyoto Encyclopedia of Genes and Genomes (KEGG) analyses [80] as previously described.

To analyze the influence of power value on the scale independence and mean connectivity, we used the function softConnectivity from the package of Weighted gene co-expression network analysis (WGCNA), with the “randomly selected genes” parameter set at 5000, other parameters set as default, and the power parameter pre-calculated by the pickSoftThreshold function of WGCNA. This function provides the appropriate soft-thresholding power for network construction by calculating the scale-free topology fit index for several powers. We next summarized the expression values using the function collapseRows implemented in the R package WGCNA. Cluster analysis was subsequently performed by flashClust [81].

DNA sample isolation, MethylRAD library preparation and sequencing

The wheat spikes of BS366 and J411 of control and cold conditions were sampled as the sampling method in the transcriptome sequencing. Genomic DNA was extracted from spike tissues using the cetyltrimethyl ammonium bromide method. The MethylRAD library was prepared by digesting genomic DNA using FspEI (New England Biolabs, Ipswich, MA, USA) at 37 °C for 45 min. The digested products were verified using 1% agarose gel. Then the digested DNA was ligated to the adaptor A and adaptor B using T4 DNA ligase (New England Biolabs, Ipswich, MA, USA). Ligation products were amplified using Phusion high-fidelity DNA polymerase (New England Biolabs, Ipswich, MA, USA). PCR was conducted using a MyCycler thermal cycler (Bio-Rad) with 16 cycles of 98℃ for 5 s, 60℃ for 20 s, 72℃ for 10 s, and a final extension of 5 min at 72℃. The target band (approx. 100 bp) was excised from an 8% polyacrylamide gel and diffused from the gel in nuclease-free water for 30 min at 37℃. DNA was PCR amplified as procedure mentioned above using 4-6 cycles. After purifying the PCR products using MinElute PCR Purification Kit (Qiagen), the barcodes were introduced by means of PCR using Phusion high-fidelity DNA polymerase (2 U/μl) (New England Biolabs, Ipswich, MA, USA). PCR products were purified using MinElute PCR Purification Kit (Qiagen) and were subjected to pair end sequencing (100-150 bp) on an Illumina Hiseq X Ten platform.

DNA methylation data analysis

Raw reads were first trimmed to remove adaptor sequences. Reads containing ambiguous base calls (N) or an excessive number of low-quality bases (more than five bases with quality less than 10) were removed. The high-quality reads were used for subsequent analysis. The Methyl-RAD sequencing tags for each sample were mapped to the reference genome (IWGSC RefSeq v1.0) using the bowtie2 software (version 2.3.4.1) [82]. The number of reads was normalized as RPM (reads per million) to quantify the methylation level of all the methylated sites. Differentially methylated sites (DMSs) were identified using DEseq with a threshold of foldchange higher than 2 and the *P*-value lower than 0.05 [39]. Genes containing differentially methylated loci were subjected to Gene Ontology (GO) and Kyoto Encyclopedia of Genes and Genomes (KEGG) analysis [79, 80].

Pyrosequencing methylation analysis

We selected the candidate genes that resulted from combining the transcriptome and MethylRAD sequencing data. The sequence of the differentially methylated region was subjected to pyrosequencing methylation sequencing. Primers for the target site were designed using PyroMark Assay Design 2.0 (Qiagen). All the primer sequences were listed in Additional file 10: Table S9. Genomic DNA was first modified with sodium bisulfite to convert the unmethylated Cs into Ts with the EpiTect Bisulfite kit (Qiagen, Germany) following the manufacturer's instructions. The modified DNA was purified using MinElute DNA spin columns (Qiagen, Germany). For each PCR reaction, 1.0 μl of bisulfite treated DNA was used in a 50 μl reaction system. These PCR products were gel-purified using a Gel Extraction Kit (Omega, USA), and then cloned into the pMD18-T vector (Takara, Dalian, China) and sequenced. At least ten clones were sequenced for each sample.

Declarations

Ethics approval and consent to participate

Not applicable.

Consent for publication

Not applicable.

Competing interests

The authors declare that they have no competing interests.

Funding

This work was financially supported by the Important Crops Genetically Modified New Germplasm Creation (KJCX20200205) and Foundation for Youths of BAAFS (Beijing Academy of Agriculture and Forestry Sciences, grant no. QNJJ202008).

Availability of data and materials

Transcriptome and the methylation sequence data for all samples can be found in the National Genomics Data Center (https://bigd.big.ac.cn/) under accession number of CRA003366.

Authors' contributions

LYJ analyzed transcriptome data and drafted the manuscript. LYJ, LD and GJ gathered the phenotype data; LYJ, GSQ, and ZCP conceived and designed research. GSQ and ZCP revised the manuscript. WYB, CZB, PBS, ZFT, CXC, GJG, YWB and TYM contributed the plant materials. All authors read and approved the final version of this manuscript.

Acknowledgements

The authors would like to express their thanks to anyone who contributed to this work.

References

1. Longin CF, Mühleisen J, Maurer HP, Zhang H, Gowda M, Reif JC: **Hybrid breeding in autogamous cereals**. *Theor Appl Genet*2012, **125**(6):1087-1096.

2. Wan X, Wu S, Li Z, Dong Z, An X, Ma B, Tian Y, Li J: **Maize Genic Male-Sterility Genes and Their Applications in Hybrid Breeding: Progress and Perspectives**. *Mol Plant*2019, **12**(3):321-342.

3. Cheng SH, Zhuang JY, Fan YY, Du JH, Cao LY: **Progress in research and development on hybrid rice: a super-domesticate in China**. *Ann Bot*2007, **100**(5):959-966.

4. Fan Y, Zhang Q: **Genetic and molecular characterization of photoperiod and thermo-sensitive male sterility in rice**. *Plant Reprod*2018, **31**(1):3-14.

5. Maan S, Carlson K, Williams N, Yang T: **Chromosomal Arm Location and Gene-Centromere Distance of a Dominant Gene for Male Sterility in Wheat 1**. *Crop Sci*1987, **27**(3):494-500.

6. Klindworth DL, Williams ND, Maan SS: **Chromosomal location of genetic male sterility genes in four mutants of hexaploid wheat**. *Crop Sci*2002, **42**(5):1447-1450.

7. Maan SS, Carlson KM, Williams ND, Yang T: **Chromosomal Arm Location and Gene-Centromere Distance of a Dominant Gene for Male Sterility in Wheat**. *Crop Sci*1987, **27**(3):494-500.

8. Maan SS, Kianian SF: **Third dominant male sterility gene in common wheat**. *Wheat Information Service*2001, **16**(Supplement s1):45-45.

9. Qi LL, Gill BS: **High-density physical maps reveal that the dominant male-sterile gene Ms3 is located in a genomic region of low recombination in wheat and is not amenable to map-based cloning**. *Theor Appl Genet*2001, **103**(6-7):998-1006.

10. Tucker EJ, Baumann U, Kouidri A, Suchecki R, Baes M, Garcia M, Okada T, Dong C, Wu Y, Sandhu A*et al*: **Molecular identification of the wheat male fertility gene Ms1 and its prospects for hybrid breeding**. *Nat Commun*2017, **8**(1):869.

11. Wang Z, Li J, Chen S, Heng Y, Chen Z, Yang J, Zhou K, Pei J, He H, Deng XW*et al*: **Poaceae-specific MS1 encodes a phospholipid-binding protein for male fertility in bread wheat**. *Proc Natl Acad Sci U S A*2017, **114**(47):12614-12619.

12. Ni F, Qi J, Hao Q, Lyu B, Luo MC, Wang Y, Chen F, Wang S, Zhang C, Epstein L*et al*: **Wheat Ms2 encodes for an orphan protein that confers male sterility in grass species**. *Nat Commun*2017, **8**:15121.

13. Xia C, Zhang LC, Zou C, Gu YQ, Duan JL, Zhao GY, Wu JJ, Liu Y, Fang XH, Gao LF*et al*: **A TRIM insertion in the promoter of Ms2 causes male sterility in wheat**. *Nat Commun*2017, **8**:15407.

14. Pallotta MA, Warner P, Kouidri A, Tucker EJ, Baes M, Suchecki R, Watson-Haigh N, Okada T, Garcia M, Sandhu A: **Wheat ms5 male-sterility is induced by recessive homoeologous A and D genome non-specific Lipid Transfer Proteins**. *The Plant J*2019.

15. Wilson ZA, Zhang DB: **From Arabidopsis to rice: pathways in pollen development**. *J Exp Bot*2009, **60**(5):1479-1492.

16. Shi J, Cui M, Yang L, Kim YJ, Zhang D: **Genetic and Biochemical Mechanisms of Pollen Wall Development**. *Trends Plant Sci*2015, **20**(11):741-753.

17. Zhang D, Luo X, Zhu L: **Cytological analysis and genetic control of rice anther development**. *J Genet Genomics*2011, **38**(9):379-390.

18. Browne RG, Iacuone S, Li SF, Dolferus R, Parish RW: **Anther Morphological Development and Stage Determination in Triticum aestivum**. *Front Plant Sci*2018, **9**:228.

19. Itoh J, Nonomura K, Ikeda K, Yamaki S, Inukai Y, Yamagishi H, Kitano H, Nagato Y: **Rice plant development: from zygote to spikelet**. *Plant Cell Physiol*2005, **46**(1):23-47.

20. Ma H: **Molecular genetic analyses of microsporogenesis and microgametogenesis in flowering plants**. *Annu Rev Plant Biol*2005, **56**:393-434.

21. Jürgens G: **Cytokinesis in higher plants**. *Annual review of plant biology*2005, **56**:281-299.

22. Livanos P, Chugh M, Müller S: **Analysis of Phragmoplast Kinetics During Plant Cytokinesis**. *Methods Mol Biol*2017, **1662**:137-150.

23. Durbarry A, Vizir I, Twell D: **Male germ line development in Arabidopsis. duo pollen mutants reveal gametophytic regulators of generative cell cycle progression**. *Plant Physiol*2005, **137**(1):297-307.

24. Manning K, Tor M, Poole M, Hong Y, Thompson AJ, King GJ, Giovannoni JJ, Seymour GB: **A naturally occurring epigenetic mutation in a gene encoding an SBP-box transcription factor inhibits tomato fruit ripening**. *Nat Genet*2006, **38**(8):948-952.

25. Lukens LN, Zhan SH: **The plant genome's methylation status and response to stress: implications for plant improvement**. *Curr Opin Plant Biol*2007, **10**(3):317-322.

26. Kim D-H, Doyle MR, Sung S, Amasino RM: **Vernalization: Winter and the Timing of Flowering in Plants**. *Annu Rev Cell Dev Bi*2009, **25**(1):277-299.

27. Zhong S, Fei Z, Chen YR, Zheng Y, Huang M, Vrebalov J, McQuinn R, Gapper N, Liu B, Xiang J*et al*: **Single-base resolution methylomes of tomato fruit development reveal epigenome modifications associated with ripening**. *Nat Biotechnol*2013, **31**(2):154-159.

28. Yong-Villalobos L, Gonzalez-Morales SI, Wrobel K, Gutierrez-Alanis D, Cervantes-Perez SA, Hayano-Kanashiro C, Oropeza-Aburto A, Cruz-Ramirez A, Martinez O, Herrera-Estrella L: **Methylome analysis reveals an important role for epigenetic changes in the regulation of the Arabidopsis response to phosphate starvation**. *Proc Natl Acad Sci U S A*2015, **112**(52):E7293-7302.

29. Min L, Li YY, Hu Q, Zhu LF, Gao WH, Wu YL, Ding YH, Liu SM, Yang XY, Zhang XL: **Sugar and Auxin Signaling Pathways Respond to High-Temperature Stress during Anther Development as Revealed by Transcript Profiling Analysis in Cotton**. *Plant Physiol*2014, **164**(3):1293-1308.

30. Ma YZ, Min L, Wang MJ, Wang CZ, Zhao YL, Li YY, Fang QD, Wu YL, Xie S, Ding YH*et al*: **Disrupted Genome Methylation in Response to High Temperature Has Distinct Affects on Microspore Abortion and Anther**

Indehiscence. *Plant Cell*2018, **30**(7):1387-1403.

31. Law JA, Jacobsen SE: **Establishing, maintaining and modifying DNA methylation patterns in plants and animals**. *Nat Rev Genet*2010, **11**(3):204-220.

32. Sijen T, Vijn I, Rebocho A, van Blokland R, Roelofs D, Mol JN, Kooter JM: **Transcriptional and posttranscriptional gene silencing are mechanistically related**. *Curr Biol*2001, **11**(6):436-440.

33. Melnyk CW, Molnar A, Bassett A, Baulcombe DC: **Mobile 24 nt small RNAs direct transcriptional gene silencing in the root meristems of Arabidopsis thaliana**. *Curr Biol*2011, **21**(19):1678-1683.

34. Strømme CB, Julkunen-Tiitto R, Krishna U, Lavola A, Olsen JE, Nybakken L: **UV-B and temperature enhancement affect spring and autumn phenology in Populus tremula**. *Plant Cell Environ*2015, **38**(5):867-877.

35. Slotkin RK, Vaughn M, Borges F, Tanurdzić M, Becker JD, Feijó JA, Martienssen RA: **Epigenetic reprogramming and small RNA silencing of transposable elements in pollen**. *Cell*2009, **136**(3):461-472.

36. Ding J, Lu Q, Ouyang Y, Mao H, Zhang P, Yao J, Xu C, Li X, Xiao J, Zhang Q: **A long noncoding RNA regulates photoperiod-sensitive male sterility, an essential component of hybrid rice**. *Proc Natl Acad Sci U S A*2012, **109**(7):2654-2659.

37. Hu J, Chen X, Zhang H, Ding Y: **Genome-wide analysis of DNA methylation in photoperiod- and thermo-sensitive male sterile rice Peiai 64S**. *BMC Genom*2015, **16**(1):102.

38. Kim D, Landmead B, Salzberg SL: **HISAT: a fast spliced aligner with low memory requirements**. *Nat Methods*2015, **12**(4):357-U121.

39. Anders S, Huber W: **Differential expression analysis for sequence count data**. *Genome Biol*2010, **11**(10):R106.

40. Wang S, Lv J, Zhang LL, Dou JZ, Sun Y, Li X, Fu XT, Dou HQ, Mao JX, Hu XL*et al*: **MethylRAD: a simple and scalable method for genome-wide DNA methylation profiling using methylation-dependent restriction enzymes**. *Open Biol*2015, **5**(11).

41. Moore PJ, Staehelin LA: **Immunogold localization of the cell-wall-matrix polysaccharides rhamnogalacturonan I and xyloglucan during cell expansion and cytokinesis inTrifolium pratense L.; implication for secretory pathways**. *Planta*1988, **174**(4):433-445.

42. Samuels AL, Giddings TH, Jr., Staehelin LA: **Cytokinesis in tobacco BY-2 and root tip cells: a new model of cell plate formation in higher plants**. *J Cell Biol*1995, **130**(6):1345-1357.

43. Lee YR, Liu B: **The rise and fall of the phragmoplast microtubule array**. *Curr Opin Plant Biol*2013, **16**(6):757-763.

44. Murata T, Sano T, Sasabe M, Nonaka S, Higashiyama T, Hasezawa S, Machida Y, Hasebe M: **Mechanism of microtubule array expansion in the cytokinetic phragmoplast**. *Nat Commun*2013, **4**:1967.

45. Otegui MS, Mastronarde DN, Kang BH, Bednarek SY, Staehelin LA: **Three-dimensional analysis of syncytial-type cell plates during endosperm cellularization visualized by high resolution electron tomography**. *Plant Cell*2001,

13(9):2033-2051.

46. Hong Z, Delauney AJ, Verma DP: **A cell plate-specific callose synthase and its interaction with phragmoplastin**. *Plant Cell*2001, **13**(4):755-768.

47. Sasabe M, Soyano T, Takahashi Y, Sonobe S, Igarashi H, Itoh TJ, Hidaka M, Machida Y: **Phosphorylation of NtMAP65-1 by a MAP kinase down-regulates its activity of microtubule bundling and stimulates progression of cytokinesis of tobacco cells**. *Genes Dev*2006, **20**(8):1004-1014.

48. Hepler PK, Jackson WT: **Microtubules and early stages of cell-plate formation in the endosperm of Haemanthus katherinae Baker**. *J Cell Biol*1968, **38**(2):437-446.

49. Hiwatashi Y, Obara M, Sato Y, Fujita T, Murata T, Hasebe M: **Kinesins are indispensable for interdigitation of phragmoplast microtubules in the moss Physcomitrella patens**. *Plant Cell*2008, **20**(11):3094-3106.

50. Jürgens G: **Plant cytokinesis: fission by fusion**. *Trends Cell Biol*2005, **15**(5):277-283.

51. Seguí-Simarro JM, Austin JR, 2nd, White EA, Staehelin LA: **Electron tomographic analysis of somatic cell plate formation in meristematic cells of Arabidopsis preserved by high-pressure freezing**. *Plant Cell*2004, **16**(4):836-856.

52. Tang Z, Zhang L, Yang D, Zhao C, Zheng Y: **Cold stress contributes to aberrant cytokinesis during male meiosis I in a wheat thermosensitive genic male sterile line**. *Plant Cell Environ*2011, **34**(3):389-405.

53. Hein S, Kostin S, Heling A, Maeno Y, Schaper J: **The role of the cytoskeleton in heart failure**. *Cardiovasc Res*2000, **45**(2):273-278.

54. Guo L, Ho CM, Kong Z, Lee YR, Qian Q, Liu B: **Evaluating the microtubule cytoskeleton and its interacting proteins in monocots by mining the rice genome**. *Ann Bot*2009, **103**(3):387-402.

55. Binarová P, Cenklová V, Procházková J, Doskocilová A, Volc J, Vrlík M, Bögre L: **Gamma-tubulin is essential for acentrosomal microtubule nucleation and coordination of late mitotic events in Arabidopsis**. *Plant Cell*2006, **18**(5):1199-1212.

56. Pastuglia M, Azimzadeh J, Goussot M, Camilleri C, Belcram K, Evrard JL, Schmit AC, Guerche P, Bouchez D: **Gamma-tubulin is essential for microtubule organization and development in Arabidopsis**. *Plant Cell*2006, **18**(6):1412-1425.

57. Smertenko A, Hewitt SL, Jacques CN, Kacprzyk R, Liu Y, Marcec MJ, Moyo L, Ogden A, Oung HM, Schmidt S*et al*: **Phragmoplast microtubule dynamics - a game of zones**. *J Cell Sci*2018, **131**(2).

58. Müller S, Smertenko A, Wagner V, Heinrich M, Hussey PJ, Hauser MT: **The plant microtubule-associated protein AtMAP65-3/PLE is essential for cytokinetic phragmoplast function**. *Curr Biol*2004, **14**(5):412-417.

59. Boruc J, Weimer AK, Stoppin-Mellet V, Mylle E, Kosetsu K, Cedeño C, Jaquinod M, Njo M, De Milde L, Tompa P*et al*: **Phosphorylation of MAP65-1 by Arabidopsis Aurora Kinases Is Required for Efficient Cell Cycle Progression**. *Plant Physiol*2017, **173**(1):582-599.

60. Caillaud MC, Lecomte P, Jammes F, Quentin M, Pagnotta S, Andrio E, de Almeida Engler J, Marfaing N, Gounon P, Abad P*et al*: **MAP65-3 microtubule-associated protein is essential for nematode-induced giant cell ontogenesis in Arabidopsis**. *Plant Cell*2008, **20**(2):423-437.

61. Hussey PJ, Hawkins TJ, Igarashi H, Kaloriti D, Smertenko A: **The plant cytoskeleton: recent advances in the study of the plant microtubule-associated proteins MAP-65, MAP-190 and the Xenopus MAP215-like protein, MOR1**. *Plant Mol Biol*2002, **50**(6):915-924.

62. Lee YR, Liu B: **Cytoskeletal motors in Arabidopsis. Sixty-one kinesins and seventeen myosins**. *Plant Physiol*2004, **136**(4):3877-3883.

63. Lee YR, Li Y, Liu B: **Two Arabidopsis phragmoplast-associated kinesins play a critical role in cytokinesis during male gametogenesis**. *Plant Cell*2007, **19**(8):2595-2605.

64. Tseng KF, Wang P, Lee YJ, Bowen J, Gicking AM, Guo L, Liu B, Qiu W: **The preprophase band-associated kinesin-14 OsKCH2 is a processive minus-end-directed microtubule motor**. *Nat Commun*2018, **9**(1):1067.

65. Goetz M, Godt DE, Guivarc'h A, Kahmann U, Chriqui D, Roitsch T: **Induction of male sterility in plants by metabolic engineering of the carbohydrate supply**. *Proc Natl Acad Sci U S A*2001, **98**(11):6522-6527.

66. Pacini E, Guarnieri M, Nepi M: **Pollen carbohydrates and water content during development, presentation, and dispersal: a short review**. *Protoplasma*2006, **228**(1-3):73-77.

67. Datta R, Chamusco KC, Chourey PS: **Starch biosynthesis during pollen maturation is associated with altered patterns of gene expression in maize**. *Plant Physiol*2002, **130**(4):1645-1656.

68. Zhang DB, Luo X, Zhu L: **Cytological analysis and genetic control of rice anther development**. *J Genet Genomics*2011, **38**(9):379-390.

69. Yu JP, Han JJ, Kim YJ, Song M, Yang Z, He Y, Fu RF, Luo ZJ, Hu JP, Liang WQ*et al*: **Two rice receptor-like kinases maintain male fertility under changing temperatures**. *P Natl Acad Sci USA*2017, **114**(46):12327-12332.

70. Zhang DS, Liang WQ, Yuan Z, Li N, Shi J, Wang J, Liu YM, Yu WJ, Zhang DB: **Tapetum degeneration retardation is critical for aliphatic metabolism and gene regulation during rice pollen development**. *Mol Plant*2008, **1**(4):599-610.

71. Qin P, Tu B, Wang Y, Deng L, Quilichini TD, Li T, Wang H, Ma B, Li S: **ABCG15 encodes an ABC transporter protein, and is essential for post-meiotic anther and pollen exine development in rice**. *Plant Cell Physiol*2013, **54**(1):138-154.

72. Quilichini TD, Samuels AL, Douglas CJ: **ABCG26-mediated polyketide trafficking and hydroxycinnamoyl spermidines contribute to pollen wall exine formation in Arabidopsis**. *Plant Cell*2014, **26**(11):4483-4498.

73. Huang MD, Chen TL, Huang AH: **Abundant type III lipid transfer proteins in Arabidopsis tapetum are secreted to the locule and become a constituent of the pollen exine**. *Plant Physiol*2013, **163**(3):1218-1229.

74. Kouidri A, Baumann U, Okada T, Baes M, Tucker EJ, Whitford R: **Wheat TaMs1 is a glycosylphosphatidylinositol-anchored lipid transfer protein necessary for pollen development**. *BMC Plant*

*Biol*2018, **18**.

75. Kouidri A, Baumann U, Okada T, Baes M, Tucker EJ, Whitford R: **Wheat TaMs1 is a glycosylphosphatidylinositol-anchored lipid transfer protein necessary for pollen development**. *BMC Plant Biol*2018, **18**(1):332.

76. Caldelari D, Wang G, Farmer EE, Dong X: **Arabidopsis lox3 lox4 double mutants are male sterile and defective in global proliferative arrest**. *Plant Mol Biol*2011, **75**(1-2):25-33.

77. Endo M, Tsuchiya T, Hamada K, Kawamura S, Yano K, Ohshima M, Higashitani A, Watanabe M, Kawagishi-Kobayashi M: **High temperatures cause male sterility in rice plants with transcriptional alterations during pollen development**. *Plant Cell Physiol*2009, **50**(11):1911-1922.

78. Iwasaki M, Paszkowski J: **Identification of genes preventing transgenerational transmission of stress-induced epigenetic states**. *Proc Natl Acad Sci U S A*2014, **111**(23):8547-8552.

79. Ashburner M, Ball CA, Blake JA, Botstein D, Butler H, Cherry JM, Davis AP, Dolinski K, Dwight SS, Eppig JT: **Gene ontology: tool for the unification of biology**. *Nature genetics*2000, **25**(1):25.

80. Kanehisa M, Goto S: **KEGG: Kyoto Encyclopedia of Genes and Genomes**. *Nucleic Acids Res*2000, **28**(1):27-30.

81. Langfelder P, Horvath S: **Fast R Functions for Robust Correlations and Hierarchical Clustering**. *J Stat Softw*2012, **46**(11).

82. Langmead B, Salzberg SL: **Fast gapped-read alignment with Bowtie 2**. *Nat Methods*2012, **9**(4):357.

Tables

Table 1 The mapping statistics of all the samples in this study

Sample	Total Reads	Total Mapped reads	Mapping Rate	Unique Mapped reads	Unique mapping rate
fBS366-1	113245958	98668138	87.13%	82899792	73.20%
fBS366-2	112097060	95441688	85.14%	82398866	73.51%
fJ411-1	116496542	94178836	80.84%	78483052	67.37%
fJ411-2	114294642	98351910	86.05%	85569280	74.87%
sBS366-1	118214624	100855918	85.32%	86617232	73.27%
sBS366-2	125833982	106080724	84.30%	91159560	72.44%
sJ411-1	104066440	89588230	86.09%	79396020	76.29%
sJ411-2	106093538	90924504	85.70%	80397514	75.78%

Table 2 The mapping statistics of all the reads from all the MethylRAD libraries

Samples	Raw Reads	Enzyme Reads	Ratio	Unique Mapped Reads	Multiple Mapped Reads	Unique Mapping ratio	Multiple Mapping ratio
sBS366.1	138,774,718	49,583,815	35.73%	4,321,361	44,579,071	8.72%	89.91%
sBS366.2	138,774,718	45,195,153	32.57%	3,824,533	40,805,978	8.46%	90.29%
fBS366.1	138,774,718	49,388,164	35.59%	4,244,368	44,521,958	8.59%	90.15%
fBS366.2	138,774,718	48,491,659	34.94%	4,227,335	43,659,713	8.72%	90.04%
sJ411.1	133,604,022	43,190,796	32.33%	3,688,005	38,865,858	8.54%	89.99%
sJ411.2	133,604,022	44,081,539	32.99%	3,729,612	39,787,159	8.46%	90.26%
fJ411.1	133,604,022	42,870,752	32.09%	3,721,482	38,571,647	8.68%	89.97%
fJ411.2	133,604,022	41,554,362	31.10%	3,570,751	37,443,799	8.59%	90.11%
All	1,089,514,960	364,356,240	33.44%	31,327,447	328,235,183	8.60%	90.09%

Figures

Figure 1

Phenotype comparison of BS366 anther and pollen under cold (sterile) and control (fertile) conditions. a The mature anther of BS366 under control condition. b Pollen grains of BS366 under control condition stained by I2-KI. c The mature anther of BS366 under cold condition. d Pollen grains of BS366 under cold condition stained by I2-KI. Bars in a and b, 2 mm; bars in c and d 100 μm

Figure 2

The microspores in fertile and sterile BS366. The microspores of fertile (a-d, i-l) and sterile BS366 (e-h, m-p). meiotic interphase (a, e), meiotic dyad (b, f), meiotic tetrad (c, g), early uninucleate stage (d, h), middle uninucleate stage (i, m), vacuolated stage (j, n), binucleate stage (k, o) and the mature pollen stage (l, p). Bars = 20 μm

Figure 3

Transverse sections of BS366 anthers from different development stages under cold and control conditions. Anthers in fertile (a-d, i-l) and sterile BS366 (e-h, m-p). pre-callose stage (a, e), meiotic stage (b, f), dyad stage (c, g), tetrad stage (d, h), the early uninucleate stage (i, m), the vacuolated stage (j, n), the binucleate stage (k, o), and the trinucleate stage. (l, p). Dy, dyad cell; E, epidermis; En, endothecium; ML, middle layer; Msp, microspores; T, tapetum; Tds, tetrads. Bars = 50 μm

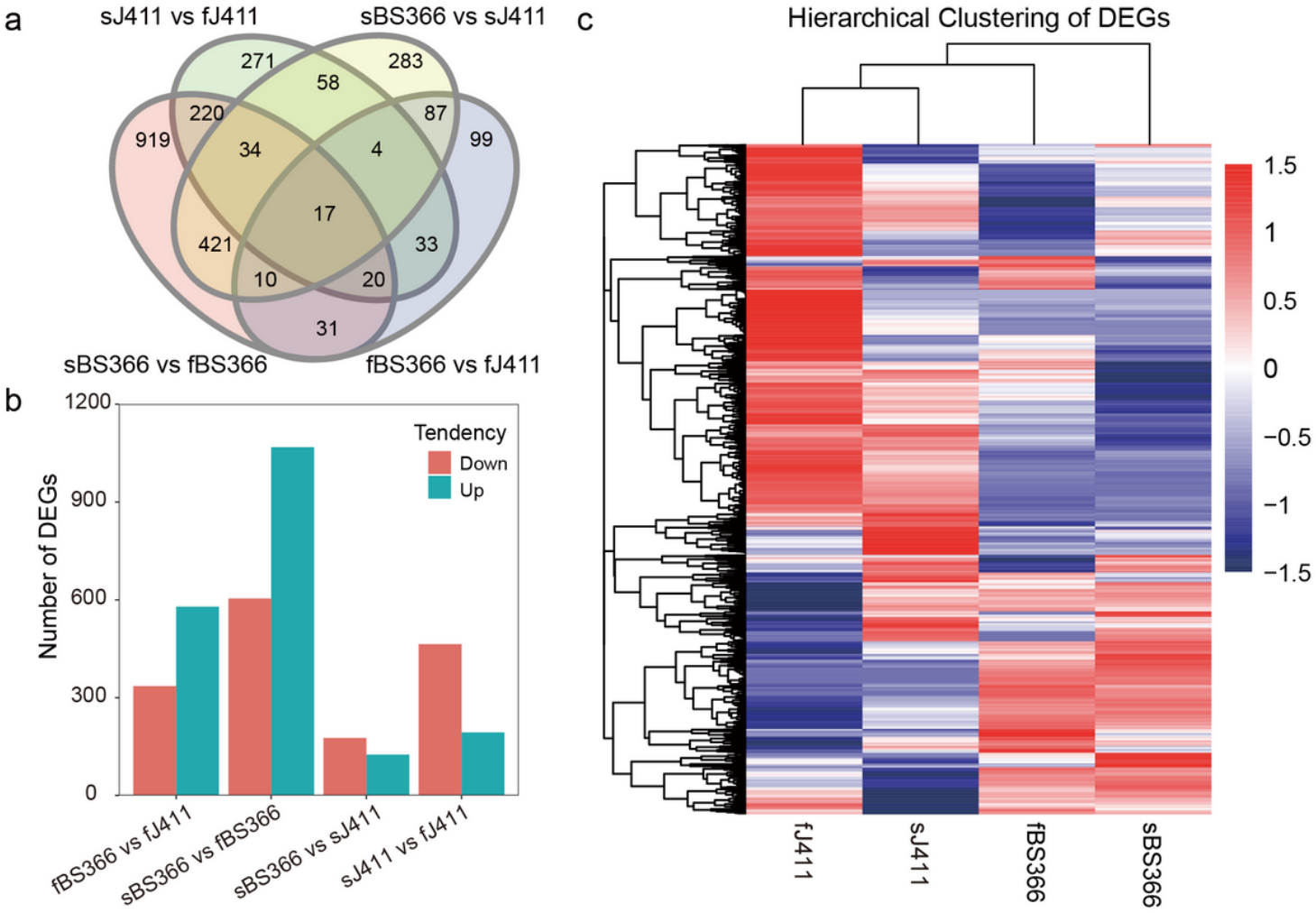

Figure 4

All the differentially expressed genes in the transcriptome sequencing data. a Venn diagram of all the differentially expressed genes in each comparison. s means sterile and f means fertile. b Number of differentially expressed genes that were up- or down-regulated in each comparison. Up means up-regulated under the sterile condition in the comparison of different conditions or in BS366 in the comparison between different samples at the same condition. c Hierarchical cluster analysis of all differentially expressed genes. The color key represents normalized log2 transformed expression of genes, with high expressed genes being red and low expressed genes being navy

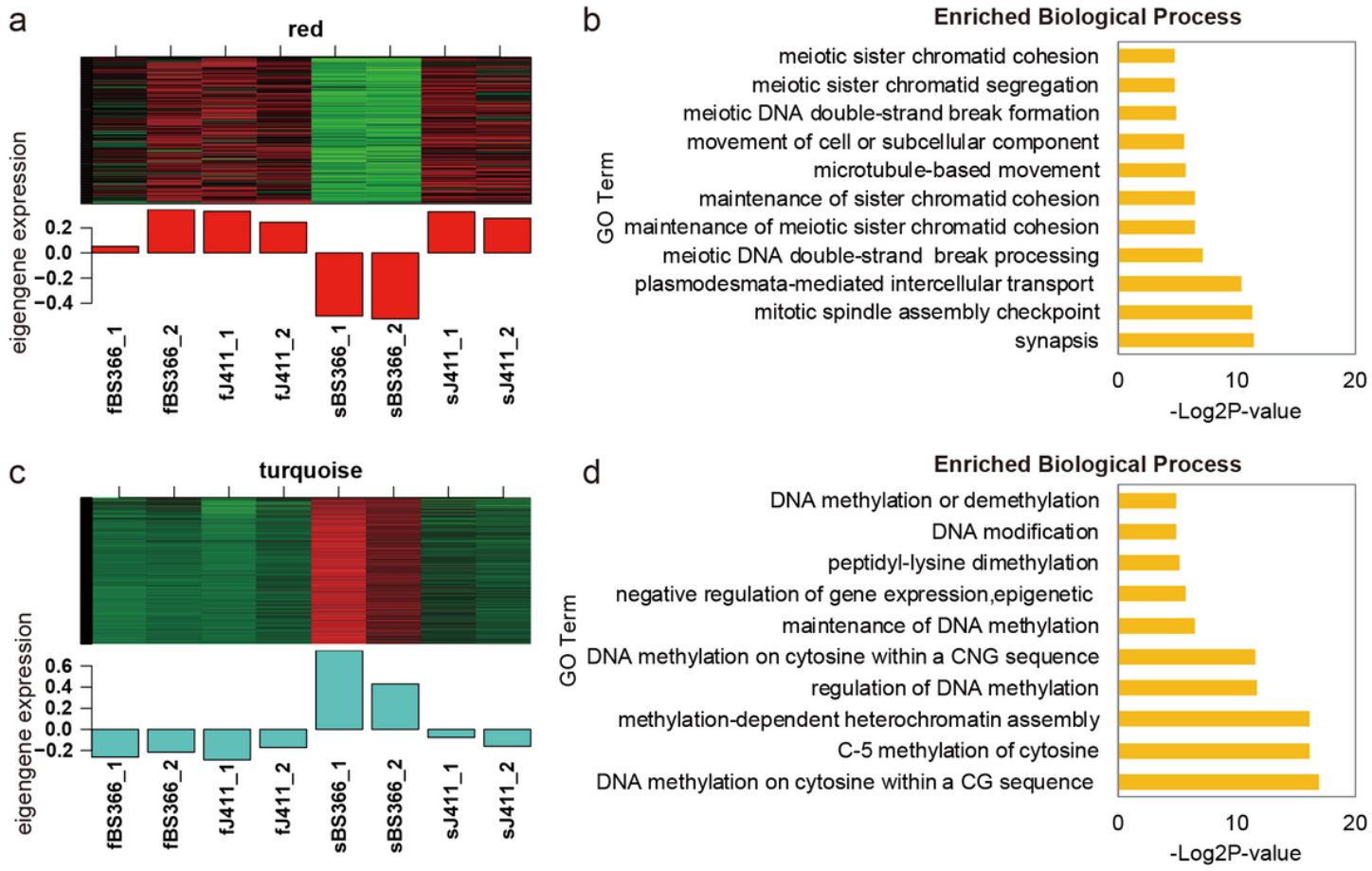

Figure 5

The expression patterns and functional analysis of genes in the co-expression modules. a Expression pattern of genes from the red module. b GO analysis of genes in the red module. c Expression pattern of genes from the turquoise module. d GO analysis of genes in the red module. In the heatmap, red indicates up-regulated genes, black indicates neutral genes, and green indicates down-regulated genes.

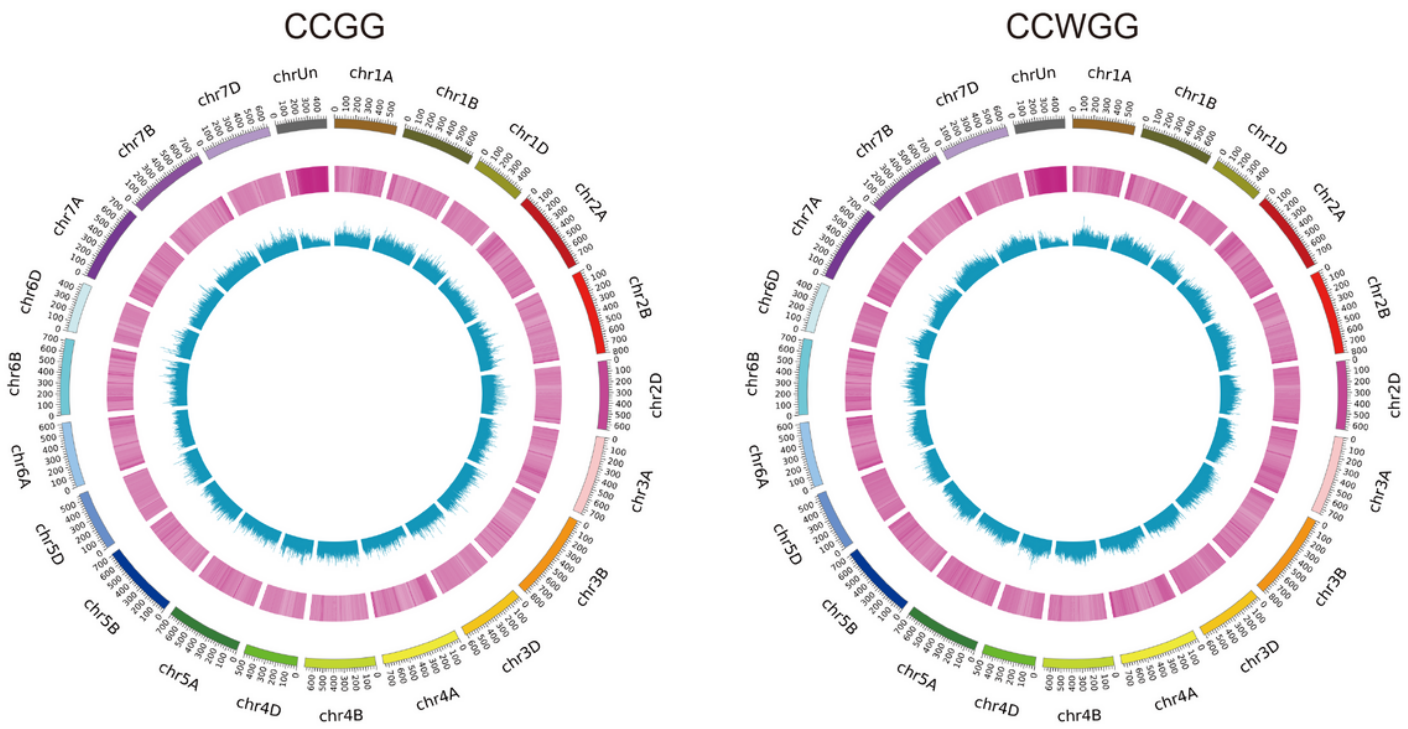

Figure 6

Genome distribution of the methylated sites in this study. Form inner outsides are histogram, heatmap, and the chromosome location of the methylated sites

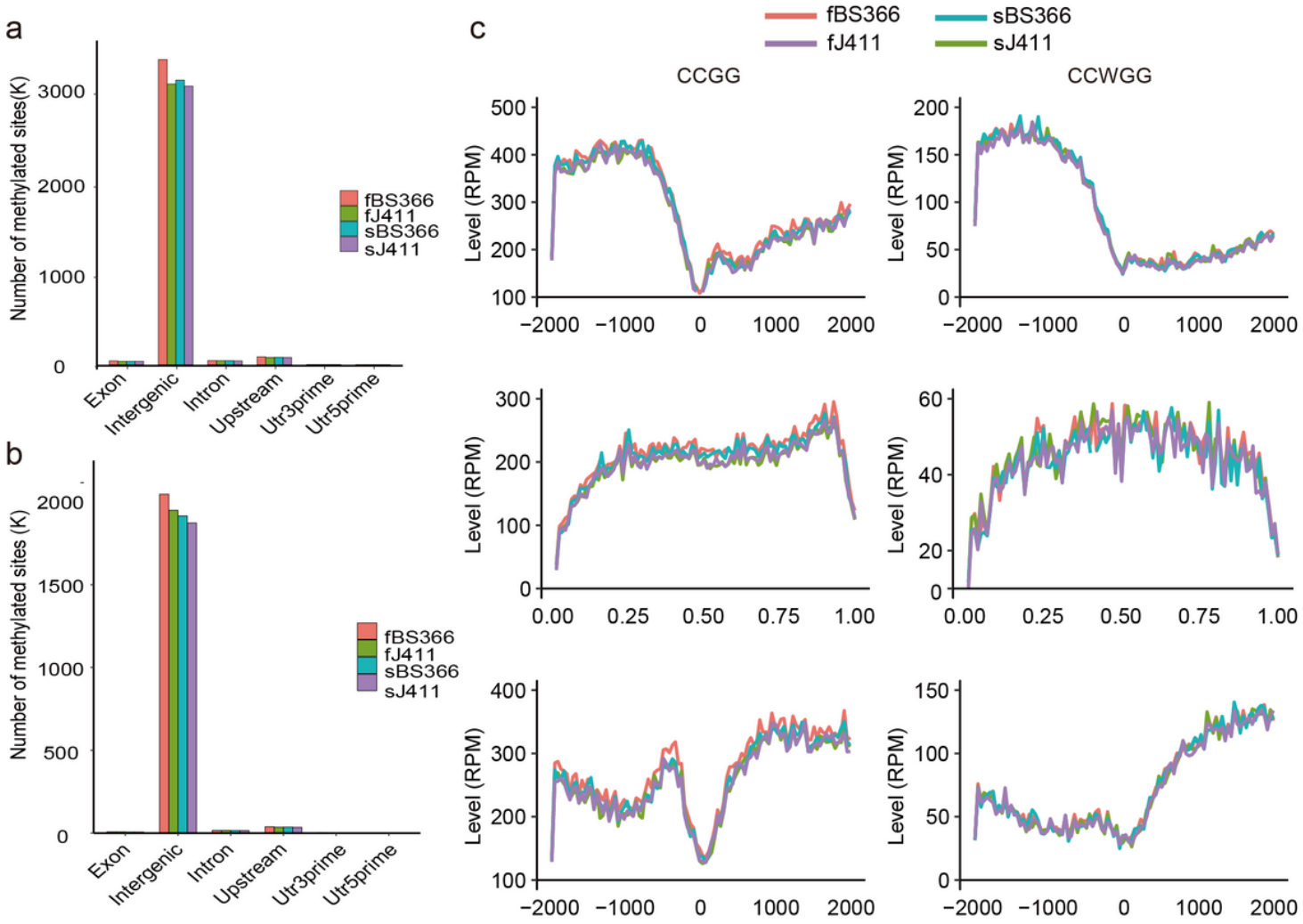

Figure 7

Genome distribution of the methylation patterns in this study. a The distribution of the CCGG sites on the genome elements for each sample. b The distribution of the CCWGG sites on the genome elements for each sample. c Analysis of the CCGG and CCWGG levels in the gene regions including promoters (-2000 bp), gene bodies and downstream regions (+2000 bp) in BS366 and J411 under cold and control conditions. Up panel, methylation level in TSS region; Middle panel, methylation level in gene body region; down panel, methylation level in TTS region. TSS, transcription start site; TTS, transcription termination sites

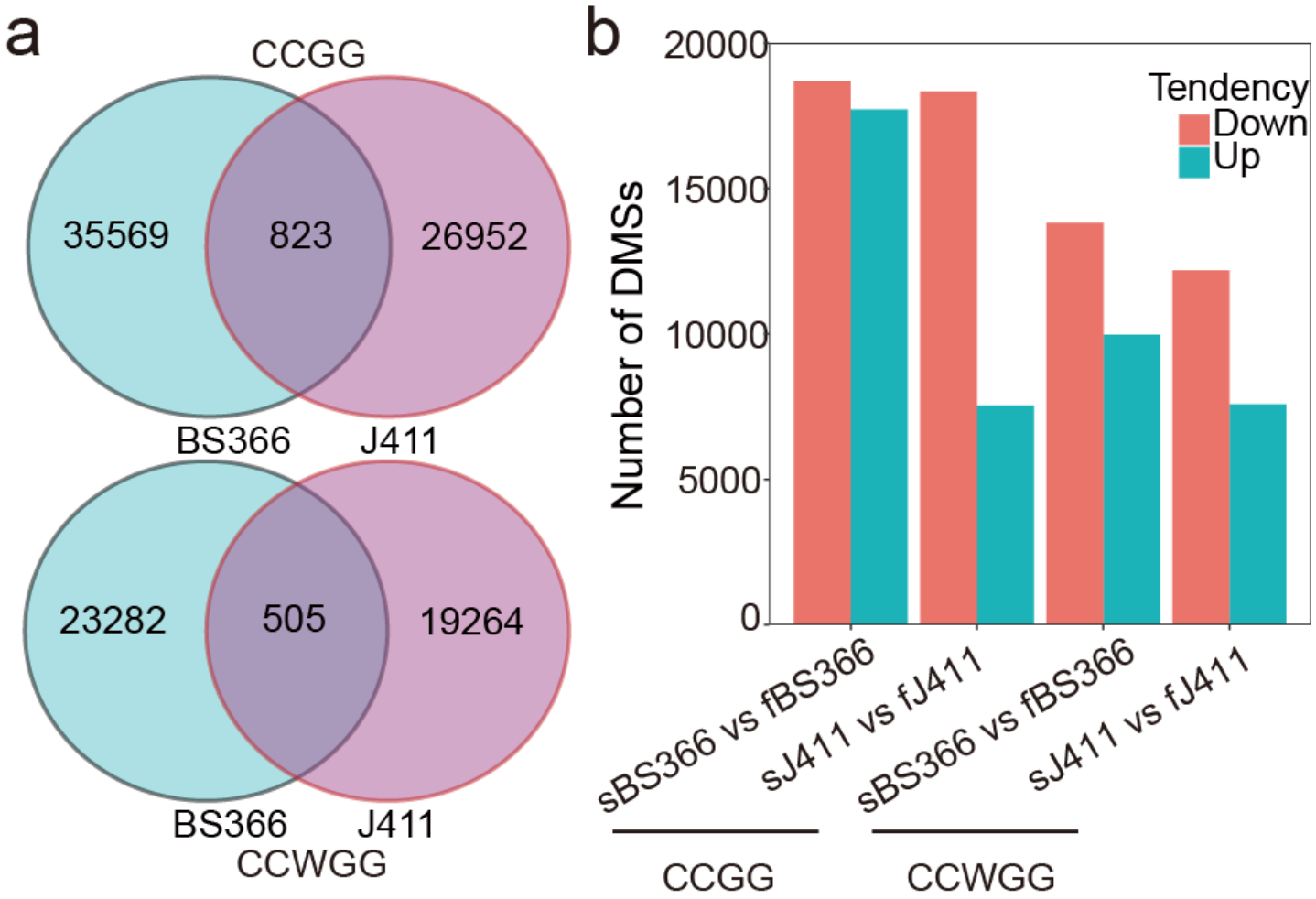

Figure 8

The differentially methylated sites in BS366 and J411 between cold and control condition. a Venn diagram analysis of the differentially methylated CCGG and CCWGG sites in BS366 and J411 under different conditions. b All the differentially methylated sites were classified as hyper- and hypo-methylated sites in BS366 or under cold condition. Up means hyper-methylated in BS366 or under cold condition; down means hypo-methylated in BS366 or under the cold condition

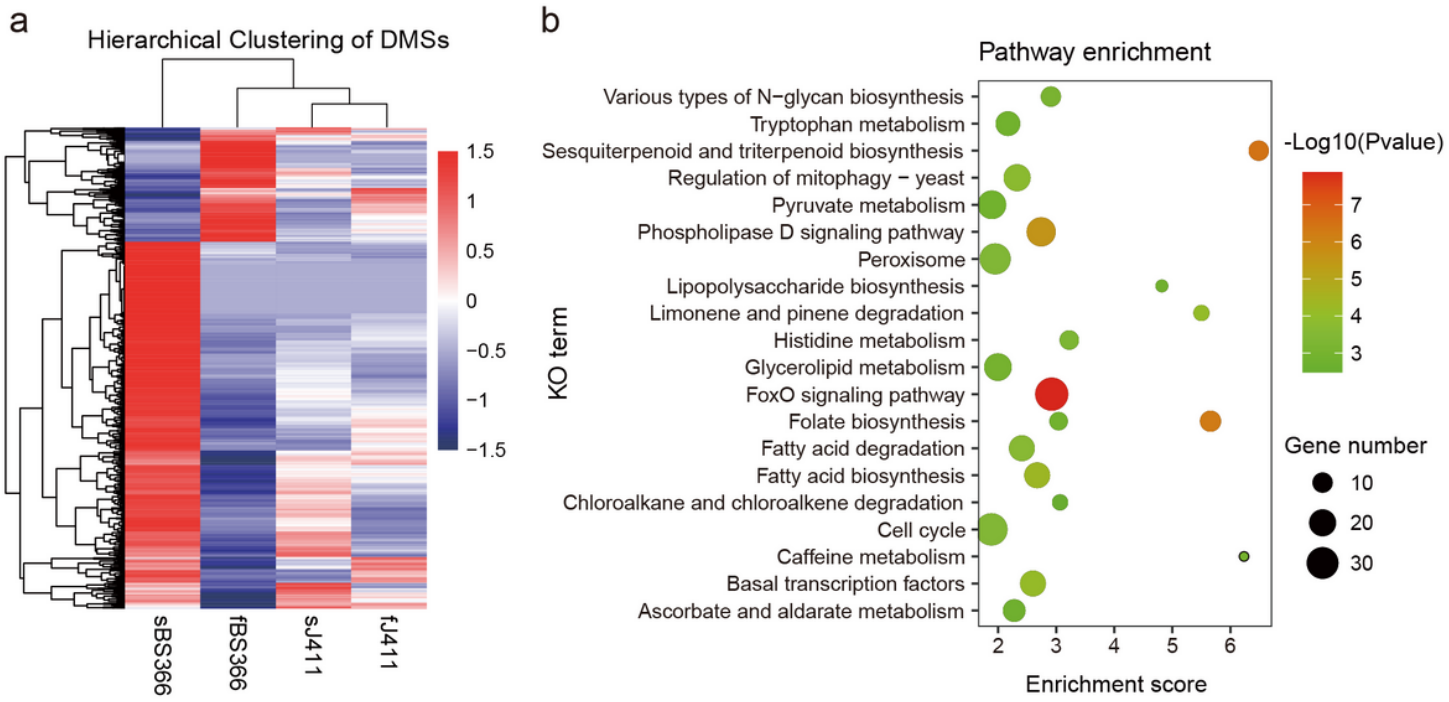

Figure 9

The exclusive DMSs in BS366 between cold and control conditions. a Expression heatmap of the exclusive DMSs in BS366 between cold and control condition. b Kyoto Encyclopedia of Genes and Genomes (KEGG) analysis of the exclusive DMSs in BS366 between cold and control conditions. The color scale means the methylation levels, red indicate high and navy indicate low methylation levels

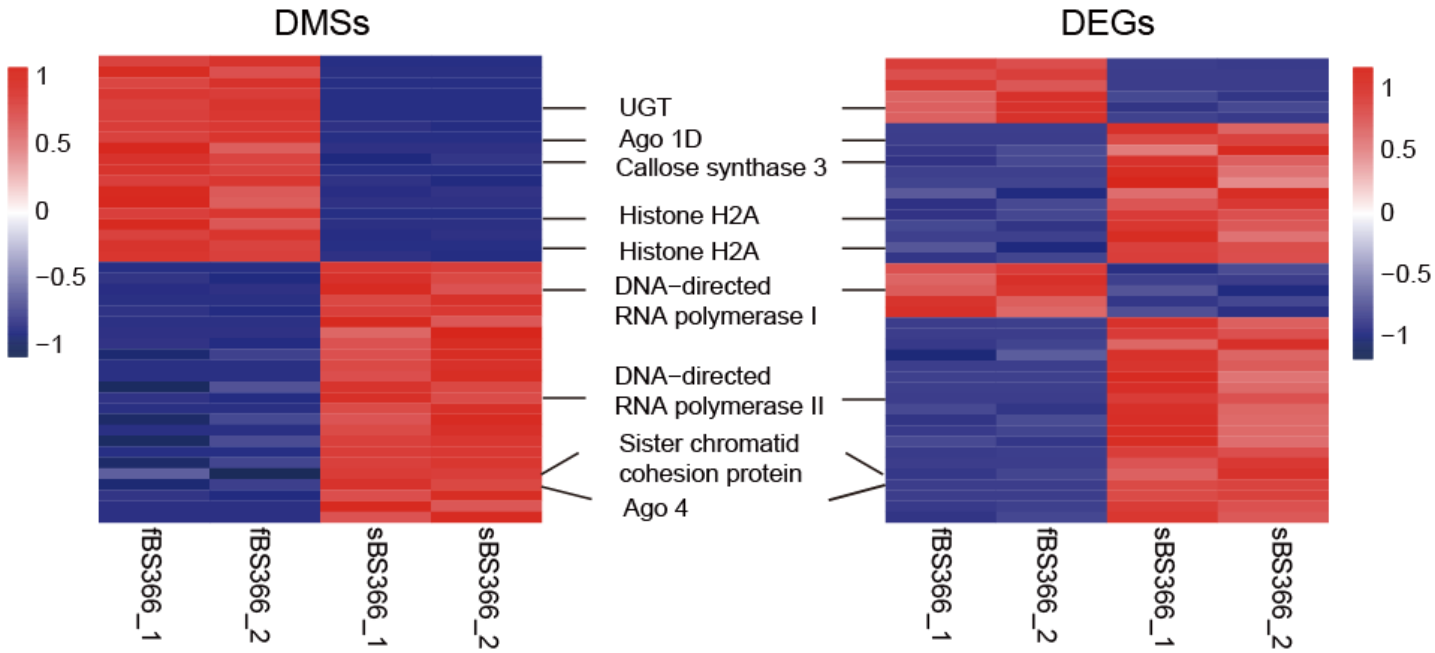

Figure 10

The expression and methylation level of genes from the integration analysis of transcriptome and methylation. Heatmap of the methylation level of DMSs in BS366 (left). Heatmap of the expression level of DEGs in BS366

(right). Red color indicates hyper-methylated or up-regulated. Navy color means hypo-methylated or down-regulated

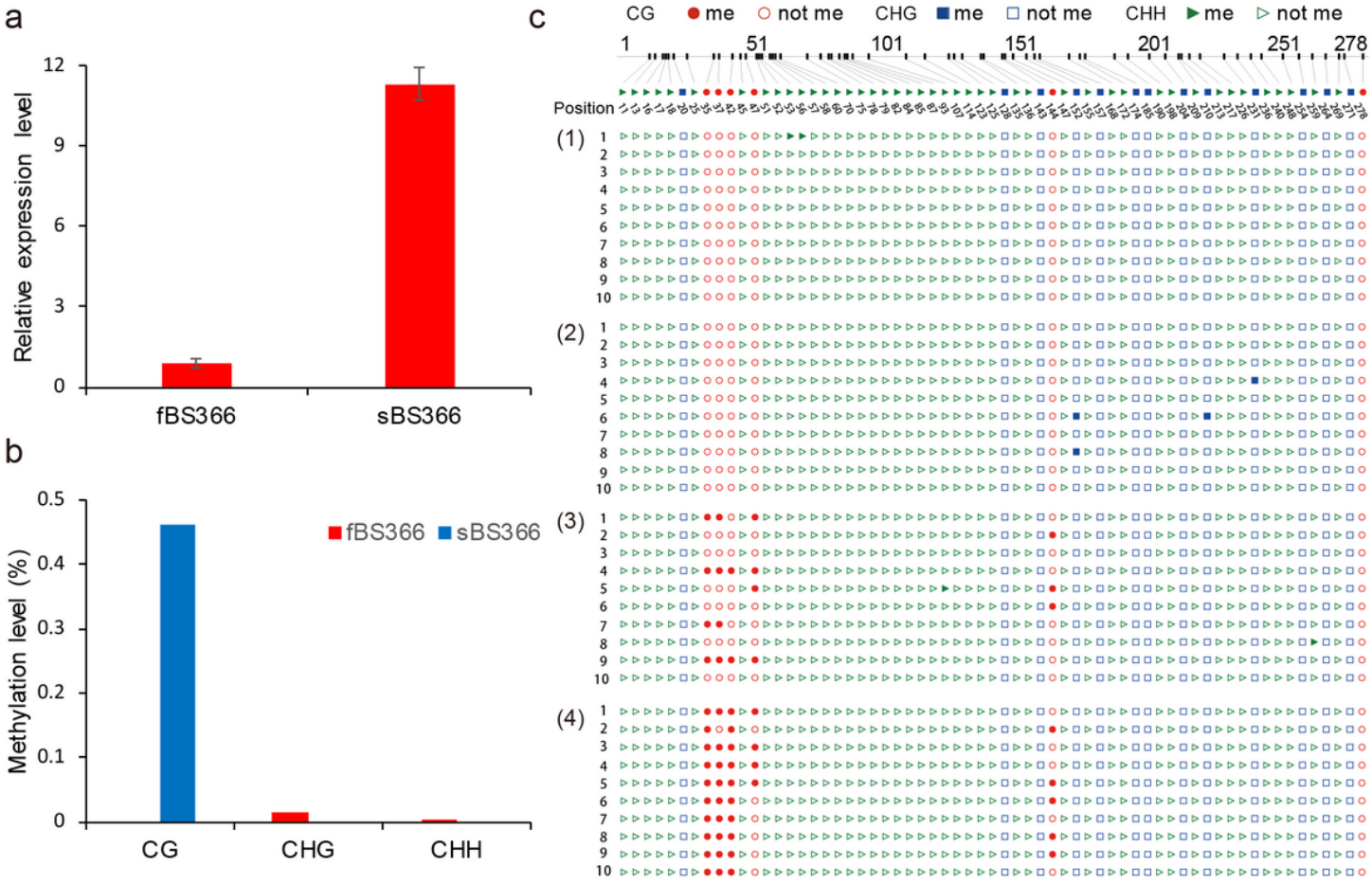

Figure 11

Expression and methylation level validation of TraesCS7A02G557400 (AGO1d) in BS366 under cold and control condition. a The expression level of BS366 under cold (sBS366) and control (fBS366) conditions. b The methylation level of the AGO1d gene in BS366 under cold and control conditions. c Bisulfite sequencing of the differentially methylated sites in the AGO1d gene. The cycle, triangle, and rectangle represent CG, CHG and, CHH context. The filled red, green and blue cycle represent methylated cytosine and the unfilled cycle, triangle and rectangle represent the unmethylated cytosine sites

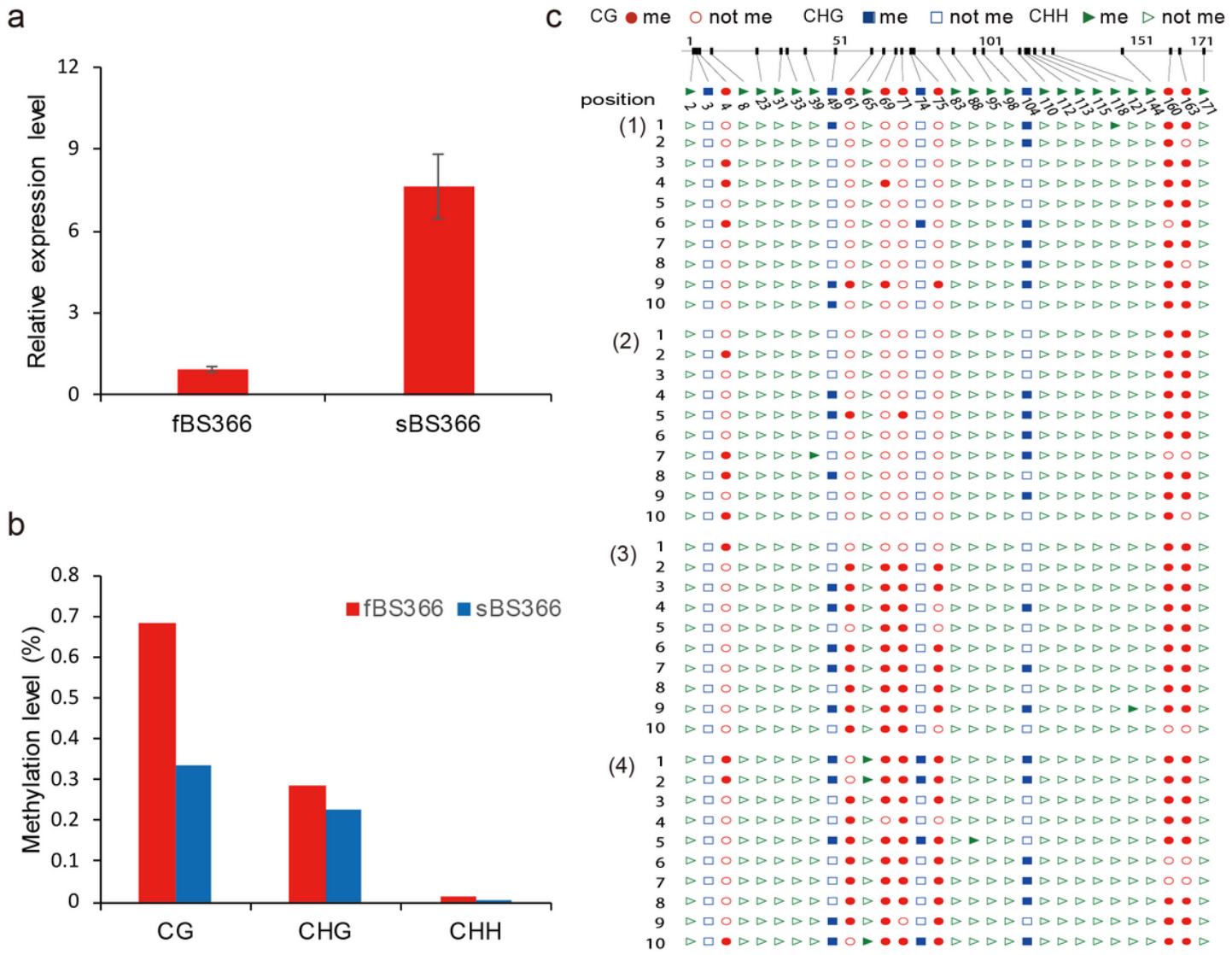

Figure 12

Expression and methylation level validation of TraesCS1B02G048900 (H2A3) in BS366 between the cold and control conditions. a The expression level of BS366 under cold (sBS366) and control (fBS366) conditions. b The methylation level of TraesCS1B02G048900 in BS366 under cold and control conditions. c Bisulfite sequencing of the differentially methylated sites in the TraesCS1B02G048900 gene. The cycle, triangle, and rectangle represent CG, CHG and CHH context. The filled red, green and blue cycle represent methylated cytosine and the unfilled cycle, triangle, and rectangle represent the unmethylated cytosine sites

Supplementary Files

This is a list of supplementary files associated with this preprint. Click to download.

- Additionalfile1.docx
- Additionalfile2TableS1.xlsx
- Additionalfile3TableS2.xlsx

- Additionalfile4TableS3.xlsx
- Additionalfile5TableS4.xlsx
- Additionalfile10TableS9.xlsx